Weathering of limestone building material by mixed sulfate solutions. Characterization of stone microstructure, reaction products and decay forms

C. Cardell[a,*], D. Benavente[b], J. Rodríguez-Gordillo[a]

[a]Department of Mineralogy and Petrology, Faculty of Science, University of Granada, Avd. Fuentenueva s/n, 18002 Granada, Spain
[b]Laboratory of Applied Petrology, Associated Unit CSIC-UA, Department of Earth and Environment Sciences, University of Alicante, 03080 Alicante, Spain

ARTICLE DATA

Article history:
Received 18 May 2007
Received in revised form
5 December 2007
Accepted 10 December 2007

Keywords:
Limestone
Sulfate solutions
Fluid transport
Microfissures
Chemical attack

ABSTRACT

This paper presents a multidisciplinary approach to characterize, at both micro- and macro-scales, the behavior of a limestone widely used as construction material in South Spain when interacting with single- and mixed sulfate solutions of differing concentrations. A salt crystallization test that depicts the reality occurring in bottom walls of buildings was used to establish the related decay morphologies and weathering mechanisms. A systematic chemical, mineralogical, petrographic and porosimetric analysis of the fresh and weathered stones, the crystallized salts, and the evolution of ion concentrations of the solutions was performed. Factors controlling the type of fluid transport within the stone and its eventual breakdown were investigated and discussed. Concentrated solutions caused the most intense damage through chemical weathering and crystallization of salts causing a disrupting effect. Simple solutions caused more salt damage than did mixed solutions. This information will enable long-term predictions of material behavior and stone deterioration in buildings.

1. Introduction

Limestone has centuries-long and worldwide tradition as a building material, with continued use in building and reconstruction activities such as replacement of damaged ashlars in monuments. Unfortunately limestone is particularly susceptible to salt weathering that ultimately causes its breaking [1]. Salt damage is considered a common risk playing a major role in the decay of natural and man-made porous materials (i.e. bricks, mortars, ceramic…) placed in civil constructions, buildings and monuments under a wide range of environmental conditions [2,3] and has significant economic and cultural implications. Thus it is critical to ascertain the parameters that control salt weathering and the operative decay processes, with an ultimate goal of mitigating potential deterioration.

Materials scientists have shown that salt attack is a part of a larger set of interrelated behaviors [4]. Addressing cultural heritage, abundant multidisciplinary contributions in the field of salts and building stone deterioration and conservation have appeared in the last decades, showing that salt damage is a complicated process topic dependent on multiple variables and physicochemical reactions operating in the substrates at micro- and nano-meter scale [5]. An additional problem is to link stone decay forms at different scales, with vital implications in monument conservation [6].

The enormous investment to save our monuments makes it essential to apply scientific knowledge of weathering processes to preserve them. Recently, great progress has been achieved in the description of factors and mechanisms controlling salt crystallization in porous media, thanks to the

* *Corresponding author*. Tel.: +34 958242725; fax: +34 958243368.
E-mail address: cardell@ugr.es (C. Cardell).

1044-5803/$ – see front matter © 2007 Elsevier Inc. All rights reserved.
doi:10.1016/j.matchar.2007.12.003

development of analytical techniques such as environmental scanning electron microscopy [7] and nuclear magnetic resonance [8]. Moreover, results from laboratory experiments [9,10], computer modeling [11] and analysis of paradigmatic case studies [12] have helped improve mitigation methods to reduce salt damage on construction and decorative materials [13].

Nonetheless numerous areas remain open for research, including the dynamics of crystal growth [14], the influence of ionic composition and solution concentrations [10,12,15], chemical modeling of phase behavior of salt mixtures [16], thermodynamic and kinetic approaches [4,17–20], and transport within the porous material [8,21,22]. Of particular interest here is the fact that most laboratory tests investigate the effect of a single salt weathering agent, whereas salts commonly occur in combination. More research is needed about how interactions between salts may increase or decrease the damage they cause individually.

This paper presents a laboratory experiment to explore the significant physicochemical changes in the microstructure and mineralogy of the building limestone from Granada (South Spain) caused by interaction with extremely harmful alkaline and alkaline earth sulfates commonly found in building materials. The results represent a multidisciplinary characterization of the fresh and salt-weathered limestones, the tested solutions and the newly formed reaction products (crystallized salts).

Conclusions are drawn regarding: i) the influence of different concentrations of single and mixed sulfate solutions on the decay morphology produced in the studied limestone, ii) the weathering processes that operate during the stone–brine interaction at micro- and macro-scales and their effect on stone breakdown, and iii) the type of fluid transport within the limestone and the factors that control it. Results from this study will facilitate modeling of material behavior and stone deterioration in civil structures and monuments.

2. Experimental Protocol

2.1. Rock Characterization

A Tortonian biomicritic limestone (calcarenite) traditionally used as building and ornamental material in Granada (South Spain) was used in the test. It is a fine-grained, buff-colored stone, composed of a variety of bioclasts and calcite cement. Fragments of quartz, feldspars and clays (i.e. smectite) are recognized in the matrix. It is very porous (mean total porosity 24.1±2.3%) with a high coefficient of capillary absorption of $753.4 \cdot 10^{-4}$ g/cm^{-2} min$^{1/2}$ (error=1.49%). Its drying rate is 0.7229 s^{-1} (slow), increasing considerably after 9 h, the capillary penetration coefficient is 0.53994 cm/min$^{1/2}$ (error=2.13%), the imbibition capacity is 18.70% and the permeability to water vapor 274.85 g/m^2·24 h. Static uniaxial compression (9.03± 2.71 MPa) and elastic module (1879±446.8 MPa) results confirm this to be a rock with low mechanical resistance [23].

2.2. Salt Crystallization Test

Our test was based on the model of salt crystallization in a rigid porous substratum proposed by Lewin [24]. Stone blocks were in permanent contact at their base with the saline solution, while low humidity was imposed above to drive the continuous capillary rise needed to compensate evaporation. The test simulates real conditions operating on foundations and low parts of walls in buildings (Fig. 1). The solution in question was poured into a 90 mm diameter, 50 mm high crystallizer and the stone block (30×30×150 mm) inserted vertically. The surface of the solution around the block was covered in heated paraffin that then solidified, allowing evaporation only through the stone. Solution was extracted from the crystallizer at fixed intervals using a needle and syringe passing through the paraffin, which allowed analysis and control of the evolution of the concentration of the remaining solution. The depth of solution in the crystallizer was 15 mm (sample height was 150 mm). The aim was to show the action of rising capillary forces in solution transport through the stone.

The test was conducted at 18–30 °C with <40% relative humidity (RH). These conditions were chosen to reproduce a natural decay situation, corresponding to values recorded in the Church of Sant Gerome (Granada, Spain) built with the same stone and a classic example of a monument affected by sulfate crystallization [12]. Extraction of solution from the crystallizer and photography were carried out from the start of the test at 20 min, 1 h, 2 h, 4 h, 15.30 h, 16 h, 19 h, 20 h, 23 h, 26.30 h, 28 h, 40.30 h and 67 h. Throughout the test a photographic record was kept of the appearance of efflorescences, evolution of crystalline habits, amount of solution in the container, drying and decay of samples. The test was judged to have finalized after 67 h for all the blocks, as no significant macroscopic changes were observed, with the exception of the block tested with the mixture of Mg-sulfate and Na-sulfate, where the first efflorescences crystallized 130 h after the start of the test. Upon conclusion, the stone blocks were removed from the crystallizers for analysis using various techniques.

2.3. Salt Solutions

Twelve single and combined saline sulfate solutions with differing degrees of concentration were chosen (Table 1). Solutions

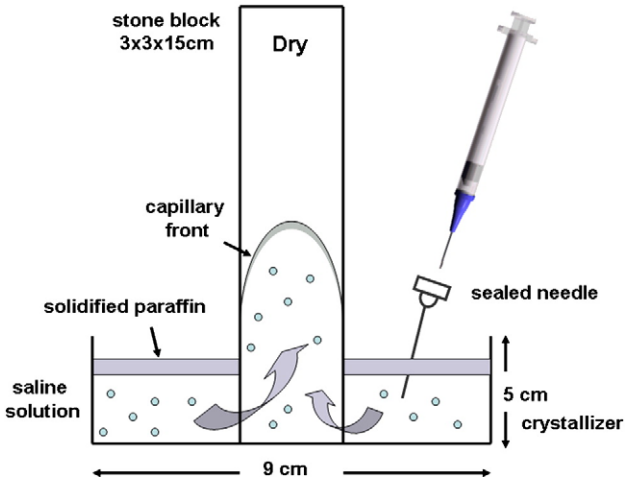

Fig. 1 – Macroscale salt weathering experiment set-up.

Table 1 – Sulfate solutions (#) used in the salt crystallization test

#	Sulfate solutions	C	V	pH	ST	ERH
5*	$CaSO_4 \cdot 2H_2O$ (gypsum)	0.24	60	5.11	25.3	–
9+	$CaSO_4 \cdot 2H_2O$		60	5.82	25.3	–
15*	$MgSO_4 \cdot 7H_2O$ (epsomite)	71.0	60	6.73	25.2	90.1
19+	$MgSO_4 \cdot 7H_2O$		60	6.54	25.3	–
27*	$Na_2SO_4 \cdot 10H_2O$ (mirabilite)	11.0	60	6.32	25.1	93.6
30+	$Na_2SO_4 \cdot 10H_2O$		60	5.80	25.3	–
48*	K_2SO_4 (arcanite)	12.2	60	6.11	25.2	97.6
44+	K_2SO_4		60	6.38	25.0	–
12*	$CaSO_4 \cdot 2H_2O + MgSO_4 \cdot 7H_2O$		30+30	6.04	20.9	–
14+	$CaSO_4 \cdot 2H_2O + MgSO_4 \cdot 7H_2O$		30+30	7.28	24.3	–
42*	$MgSO_4 \cdot 7H_2O + Na_2SO_4 \cdot 10H_2O$		30+30	6.89	24.3	–
43+	$MgSO_4 \cdot 7H_2O + Na_2SO_4 \cdot 10H_2O$		30+30	6.10	20.1	–

*: concentrated solutions; +: diluted solutions (1/50); –: unknown values. C: concentration (g/100 ml in cold water); V: Volume (ml in crystallizer); pH at ±20 °C; ST: Solution Temperature (°C); ERH: Equilibrium Relative Humidity of the salts at 20 °C. Data from CRC Handbook of Chemistry and Physics [42]. pH measured by the authors (Eutech 1500).

(Panreac, analytical grade) of combined salts were obtained by mixing equal volumes of saturated solutions of each of the component parent salts. Saturated salt solutions were used to better identify their weathering effects on the calcarenite, and diluted solutions (1/50 proportion) since they better represent the reality of monuments. Key properties of the simple concentrated sulfate solutions are shown in Table 2.

2.4. *Analytical Techniques*

Before and after the test the blocks were weighed and ultrasonic transmission speeds measured (direct transmission measurement method) following NORMAL 22/86 [25]. To evaluate the binding or disintegrating effect of the different solutions on the stones they were not water cleaned, therefore subflorescences were not removed, and instead efflorescences were manually eliminated. Cylindrical transducers (100 kHz) were used, with an elastomer as the separation medium between sensor and stone. Three measurements were taken along the blocks' maximum length, providing the mean value and standard deviation. The equipment used was a STEINKAMP model BP V.

Table 2 – Physical properties of concentrated sulfate solutions (20 °C)

Sulfate solutions	Surface tension (mN/m)	F (rhe)	Kv* (cP)	Kv¥ (cP)	Kv§ (cP)
$CaSO_4 \cdot 2H_2O$	–	–	–	–	–
$MgSO_4 \cdot 7H_2O$	73.78	54.69	1.144	1.657	4.177
$Na_2SO_4 \cdot 10H_2O$	74.15	71.95	1.065	1.274	1.871
K_2SO_4	–	88.32	1.010	1.048	–

Fluidity (F); Kinematic viscosity (Kv): ratio of dynamic viscosity to mass density; *: at 3%; ¥: at 10%, §: at 22% (g of anhydrous solute/100 g solution);–: unknown values. From CRC Handbook of Chemistry and Physics [42,43].

Following the intervals specified in *salt crystallization test*, solution samples were extracted from the crystallizer to determine the evolution of ion concentrations as an indication of the type of fluid transport operating inside the calcarenite. One ml of solution was extracted and dilutedd in 100 ml of distilled water. The cations (Mg^{2+}, Ca^{2+}, K^+ and Na^+) were determined by Inductively Coupled Plasma (ICP) (Leeman Labs PS series) and the anions (Cl^-, NO_3^- and SO_4^{2-}) by Ion Chromatography (IC) (Dionex DX 300), with further dilutions necessary up to 1/5000 to adjust to the detection range of the analytic techniques applied. Although the dilutions are very high, as too are the possible errors in measurement, we should emphasize that our interest lay not so much in the absolute values of ion concentration but in their variation patterns.

The efflorescence habits were examined using a binocular microscope with photographic camera (Olympus SZH10), and later on identified using X-Ray Diffraction (XRD) (Philips PW 1710). The petrographic characteristics of the calcarenite and the habit and precipitation place of the salts were examined under Optical Microscope (OM) (Carl Zeiss Jenapol U). Thin sections were prepared with ethanol (99.9% pure alcohol) to avoid dissolution of the salts. The sections were taken at different heights on the blocks, depending on the presence of efflorescences: when present, sections were taken from the boundary zone between affected and unaffected areas of the stone, which varied for each block tested; whereas in their absence, the sections were taken from the middle zone of the stone. In all cases the sections were taken from the inner part of the stone, with the exception of block no. 27 where it was taken from the outside.

The habit and chemical composition of the salts were analyzed by scanning electron microscopy (SEM) using a Zeiss DSM950 equipped with a Link energy-dispersive X-Ray (EDX) microanalytical system (QX2000) on small chips of unprepared rock, as the thin sections could not be used due to their lack of polishing. Analyses were carried out with no beryllium window at low intensity voltage (10–15 Kv). The pore system before and after treatments was evaluated by Mercury Porosimetry (MP). The samples were extracted following the same procedure as for the thin sections and measurements made under low (PASCAL 140) and high (PASCAL 240) pressure on Carlo Erba equipment.

Table 3 – Variation in mass (g) of the blocks before (B) and after (A) introducing the solutions (#)

#	Sulfate solutions	B	A
5*	$CaSO_4 \cdot 2H_2O$	162.29	165.45
9+	$CaSO_4 \cdot 2H_2O$	165.77	165.84
15*	$MgSO_4 \cdot 7H_2O$	163.38	176.93
19+	$MgSO_4 \cdot 7H_2O$	150.29	153.68
27*	$Na_2SO_4 \cdot 10H_2O$	155.67	157.70
30+	$Na_2SO_4 \cdot 10H_2O$	164.78	164.91
48*	K_2SO_4	157.63	174.25
44+	K_2SO_4	157.77	157.88
12*	$CaSO_4 \cdot 2H_2O + MgSO_4 \cdot 7H_2O$	153.25	163.38
14+	$CaSO_4 \cdot 2H_2O + MgSO_4 \cdot 7H_2O$	153.85	154.08
42*	$MgSO_4 \cdot 7H_2O + Na_2SO_4 \cdot 10H_2O$	158.16	175.68
43+	$MgSO_4 \cdot 7H_2O + Na_2SO_4 \cdot 10H_2O$	151.50	151.75

*: concentrated solutions; +: diluted solutions (1/50).

3. Results

3.1. *Macroscale Observation of Salt Crystallization*

The saline solutions have differing effects on the calcarenite depending on their degree of concentration and whether they are simple or mixed solutions. All the diluted solutions have similar effects on the stone, none of them causing efflorescences, with the exception of the Na-sulfate solution, which caused abundant crystallization of loose aggregates 26 h after the start of the test. There was no appreciable variation in the mass of the blocks before and after testing, during which all were completely soaked between 15 and 23 h and completely dried after 3 to 6 days. The solutions were almost entirely absorbed by the calcarenite.

By contrast, the concentrated solutions had different effects according to their composition. After the test all the blocks had increased in mass (Table 3) and approximately 75% of the initial solution volume remained in the crystallizers. All the concentrated solutions (except Ca-sulfate) caused efflorescences in the form of crusts, which appeared at different times and reached different heights on the blocks according to the nature of the solution tested. The Mg-sulfate solution caused a hard crust only on the lower part of the wet stone 40 h after beginning the test, and this was also the block with most vertical cracks, especially near the top where bursting was visible (Fig. 2). The K-sulfate solution created a hard film up to a height of 80 mm on which whiskers crystallized 90 h after the start of the test. The Na-sulfate solution caused loss of material through sanding off and abundant efflorescences 20 to 23 h into the test, which grew with time. From the paraffin surface up to 80 mm a hard crust crystallized, between 80 and 130 mm granular and acicular aggregates precipitated and between 130 and 150 mm loose efflorescences and whiskers precipitated. Over time all the efflorescences became powdery. As regards the mixed solutions, the diluted solutions did not cause efflorescences and the concentrated ones produced a thin crust only perceptible by touch 40 h after the start of the test.

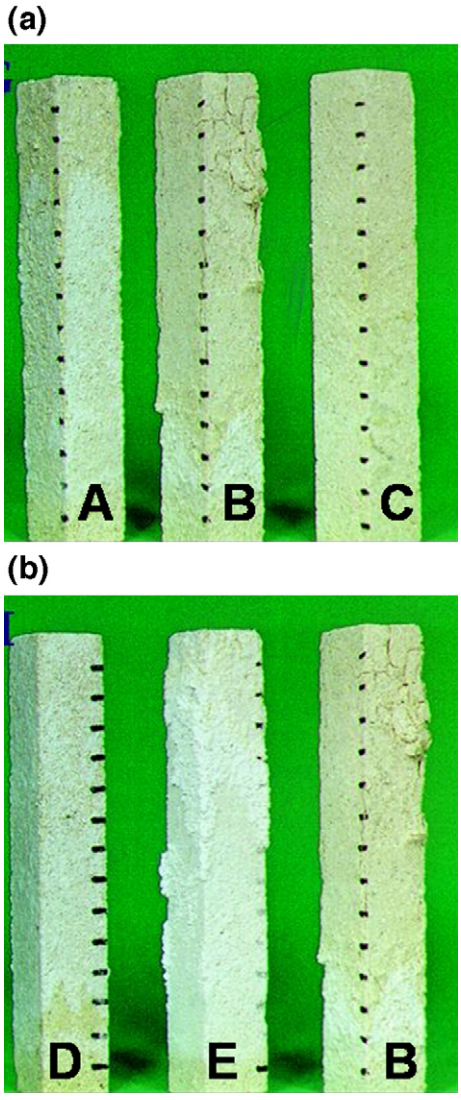

Fig. 2 – Macroscale view of the blocks: (A) after subjected to $MgSO_4 \cdot 7H_2O$ and $CaSO_4 \cdot 2H_2O$ solution; (B) after subjected to $MgSO_4 \cdot 7H_2O$ solution. Notice the intense fissuring and bursting in the upper part of the block; (C) after subjected to $CaSO_4 \cdot 2H_2O$ solution. Note the good conservation of the stone showing neither efflorescences nor fissures; (D) after subjected to $Na_2SO_4 \cdot 10H_2O$ and $MgSO_4 \cdot 7H_2O$ solution; (E) after subjected to $Na_2SO_4 \cdot 10H_2O$ solution. Observe the abundant efflorescences in the block. All are concentrated solutions.

3.2. *Evolution of the Saline Solution Concentrations*

Table 4 shows the results of the chemical analysis of the concentration of the sulfate anions, and Table 5 the results of the cations measured in the test solutions. The concentration of

Table 4 – Concentration values of the SO_4^{2-} (mg/l) in the solutions (#)

#	SO_4^{2-}	#	SO_4^{2-}
5-0*	0.12	9-0+	0.37
5-1	0.15	9-1	1.04
5-2	0.12	9-2	1.40
5-3	0.16	9-3	2.44
5-4	0.11	19-0+	0.10
15-0*	1.81	19-1	1.91
15-1	1.90	19-2	2.07
15-2	1.87	19-3	1.93
15-3	1.78	30-0+	0.11
15-4	1.75	30-1	0.79
27-0*	0.77	30-2	0.78
27-2	0.77	30-3	0.83
27-3	0.76	30-4	0.82
27-4	0.74	44-0+	0.36
48-0*	1.30	44-1	1.11
48-1	1.10	44-2	1.06
48-2	1.06	44-3	0.82
48-3	1.04		

The numbers added behind the hyphen indicate check times of the solutions. 0: 20 min; 1: 1 h; 2: 2 h; 3: 4 h; 4: 15.3 h; Solutions: 5 and 9: $CaSO_4 \cdot 2H_2O$; 15 and 19: $MgSO_4 \cdot 7H_2O$; 27 and 30: $Na_2SO_4 \cdot 10H_2O$; 44 and 48: K_2SO_4; *: concentrated solutions; +: diluted solutions (1/50).

Table 5 – Concentration values of the cations (mg/l) contained in the sulfate solutions (#)

#	Mg^{2+}	Ca^{2+}	#	Mg^{2+}	Ca^{2+}	K^+	Na^+
5-1*		5.60	27-0*		0.09		2.5
5-2		5.60	27-1		0.10		2.9
5-3		5.90	27-2		0.10		2.8
9-0+		0.26	27-3		0.10		2.8
9-1		0.69	27-4		0.10		2.8
9-2		0.63	30-0+		0.2		3.3
9-3		1.14	30-1		0.5		2.3
12-0*	4.0	2.50	30-2		0.5		2.5
12-1	5.2	2.90	30-3		0.75		2.5
12-2	4.6	3.30	30-4		0.9		2.6
12-3	4.8	3.70	42-0*	4.1	0.6		1.2
14-0+	2.3	0.21	42-1	4.4	1.3		0.9
14-1	4.0	0.50	42-2	4.3	0.1		0.9
14-2	4.0	0.49	42-3	4.1	0.1		0.8
14-3	4.1	1.60	43-0+	2.2	0.1		1.3
15-0*	9.4	0.11	43-1	3.5	0.2		1.1
15-1	9.6	0.79	43-2	3.6	0.38		0.9
15-2	9.5	0.14	43-3	3.6	0.5		1.0
15-3	9.1	0.16	44-0+		0.27	10.4	
15-4	9.0	0.15	44-1		0.29	4.6	
19-0+	8.0	0.99	44-2		0.26	4.7	
19-1	9.5	0.39	44-3		0.20	4.5	
19-2	9.4	0.56	48-0*		0.5	8.4	
19-3	9.6	1.09	48-1		0.1	7.1	
			48-2		0.1	7.1	
			48-3		0.1	6.8	
			48-4		0.1	6.4	

The numbers added behind the hyphen indicate check times of the solutions as in Table 4; Solutions 5 and 9: $CaSO_4{\cdot}2H_2O$; 12 and 14: $CaSO_4{\cdot}2H_2O + MgSO_4{\cdot}7H_2O$; 15 and 19: $MgSO_4{\cdot}7H_2O$; 27 and 30: $Na_2SO_4{\cdot}10H_2O$; 42 and 43: $MgSO4{\cdot}7H_2O + Na_2SO_4{\cdot}10H_2O$; 44 and 48: K_2SO_4; *: concentrated solutions; +: diluted solutions (1/50).

the sulfate ion remains constant in the concentrated solutions, whereas it increases in the diluted solutions. Cation concentration is likewise constant in the concentrated solutions; however, in the diluted solutions the values are dispersed, suggesting a particular evolution pattern for each cation in the different test solutions. The Mg^{2+} concentration increases slightly in all solutions containing Mg-sulfate and the Na^+ concentration remains practically constant in all solutions containing Na-sulfate. The K^+ concentration falls slightly in both the concentrated and diluted K-sulfate solutions. Finally, the concentration of the Ca^{2+} ion remains constant in all the concentrated solutions, but shows a slight increase in the diluted solutions.

Table 6 – Mean values and standard deviation of ultrasonic transmission velocity (m/s) for blocks before (B) and after (A) introducing the sulfate solutions (#)

#	B	A	#	B	A
5*	2929±102	–	19+	2918±94	2982±79
9+	2877±85	–	27*	2901±84	–
12*	2939±66	–	30+	2928±64	3010±79
14+	2892±87	2961±49	44+	2870±94	–
15*	2982±110	–	48*	2887±49	2736±79

Solutions 5 and 9: $CaSO_4{\cdot}2H_2O$; 12 and 14: $CaSO_4{\cdot}2H_2O + MgSO_4{\cdot}7H_2O$; 15 and 19: $MgSO_4{\cdot}7H_2O$; 27 and 30: $Na_2SO_4{\cdot}10H_2O$; 44 and 48: K_2SO_4; *: concentrated solutions; +: diluted solutions; –: no coherent ultrasonic response.

Table 7 – Mineralogical composition of the efflorescences in the blocks after introducing the sulfate solutions (#)

#	Sulfate solutions	Location, growth morphology	Efflorescences
12*	$CaSO_4{\cdot}2H_2O + MgSO_4{\cdot}7H_2O$	Thin and fragile yellowish crust up to mm 120	$MgSO_4{\cdot}6H_2O$
15*	$MgSO_4{\cdot}7H_2O$	Hard yellowish crust above the paraffin surface up to mm 50	$MgSO_4{\cdot}6H_2O$, $MgCO_3{\cdot}3H_2O$, $CaSO_4{\cdot}2H_2O$
27*	$Na_2SO_4{\cdot}10H_2O$	Opaque loose efflorescences all over the block	Na_2SO_4
30+	$Na_2SO_4{\cdot}10H_2O$	Yellowish loose efflorescences all over the block	Na_2SO_4
42*	$MgSO_4{\cdot}7H_2O + Na_2SO_4{\cdot}10H_2O$	Mm = 20–70. Thin, hard and transparent crust	$MgSO_4{\cdot}6H_2O$, Na_2SO_4, $CaSO_4{\cdot}2H_2O$, $MgSO_4{\cdot}7H_2O$
42*	$MgSO_4{\cdot}7H_2O + Na_2SO_4{\cdot}10H_2O$	Mm = 100–150. Crust made of hard, opaque granular crystals	$MgSO_4{\cdot}6H_2O$, Na_2SO_4, $MgSO_4{\cdot}7H_2O$

*: concentrated solutions; +: diluted solutions; $MgSO_4{\cdot}6H_2O$: hexahydrite; $MgCO_3{\cdot}3H_2O$: nesquehonite; Na_2SO_4: thenardite.

Table 8 – Optical microscopy study of the calcarenites tested with the sulfate solutions (#)

#	Sulfate solutions	Observations
5*	$CaSO_4{\cdot}2H_2O$	Scarce subflorescences. Low carbonate cement dissolution
9+	$CaSO_4{\cdot}2H_2O$	Scarce subflorescences. Intergranular fissures sub-parallel to the surface
12*	$CaSO_4{\cdot}2H_2O + MgSO_4{\cdot}7H_2O$	Efflorescences. Cement and bioclast dissolution. Scarce intragranular fissures
14+	$CaSO_4{\cdot}2H_2O + MgSO_4{\cdot}7H_2O$	Very scarce subflorescences. Abundant intragranular fissures. Carbonate cement dissolution
15*	$MgSO_4{\cdot}7H_2O$	Subflorescences, Scarce inter- and intragranular fissures
19+	$MgSO_4{\cdot}7H_2O$	Efflorescences and subflorescences. Carbonate cement dissolution. Moderate development of intragranular fissures
27*	$Na_2SO_4{\cdot}10H_2O$	Abundant efflorescences and subflorescences in pores of different size. Carbonate cement dissolution. Scarce intragranular fissures
30+	$Na_2SO_4{\cdot}10H_2O$	Efflorescences and scarce subflorescences. Carbonate cement dissolution. Abundant intragranular fissures
42*	$MgSO_4{\cdot}7H_2O + Na_2SO_4{\cdot}10H_2O$	Efflorescences and subflorescences. Scarce intragranular fissures
43+	$MgSO_4{\cdot}7H_2O + Na_2SO_4{\cdot}10H_2O$	Scarce salts. Intense intragranular fissuring
48*	K_2SO_4	Efflorescences and scarce subflorescences. Carbonate cement dissolution. Slight fissuring
44+	K_2SO_4	Lack of salts. Very slight fissuring

*: concentrated solutions; +: diluted solutions.

3.3. *Ultrasonic Transmission Velocity*

Table 6 shows the results of the ultrasonic transmission velocity in the blocks before and after the salt crystallization test. The ultrasonic velocity range in the unaltered stone was 2870±94 to 2982±110 m s^{-1}. After the test we found that in general there was no coherent ultrasonic response in the blocks tested with concentrated solutions, except for the one treated with K-sulfate, where a small decrease in transmission velocity was noted. The blocks tested with diluted solutions showed scarcely any variation in ultrasonic velocity from the untreated stones, as the differences in measurement fell within the standard deviation.

3.4. *X-Ray Diffraction*

Table 7 presents the mineralogical composition of the efflorescences and their habits and location on the blocks. The results show that the efflorescences are less hydrated than the corresponding soluble salts used in the test. Thus, hexahydrite ($MgSO_4·6H_2O$) precipitated when the solution tested was epsomite ($MgSO_4·7H_2O$) and thenardite (Na_2SO_4) precipitated from the saline solution of mirabilite ($NaSO_4·10H_2O$). The concentrate solutions containing Mg-sulfate caused precipitation of nesquehonite ($MgCO_3·3H_2O$) and gypsum ($CaSO_4·2H_2O$) on the calcarenite, as well as epsomite and hexahydrite. No gypsum efflorescences were identified on any of the stones tested with solutions containing gypsum. Both the concentrate and diluted solutions with a high Na-sulfate content only caused precipitation of thenardite.

3.5. *Optical Microscopy*

Table 8 shows the results of the petrographic study after the test. All the concentrated solutions caused precipitation of salts (subflorescences and efflorescences), encouraged

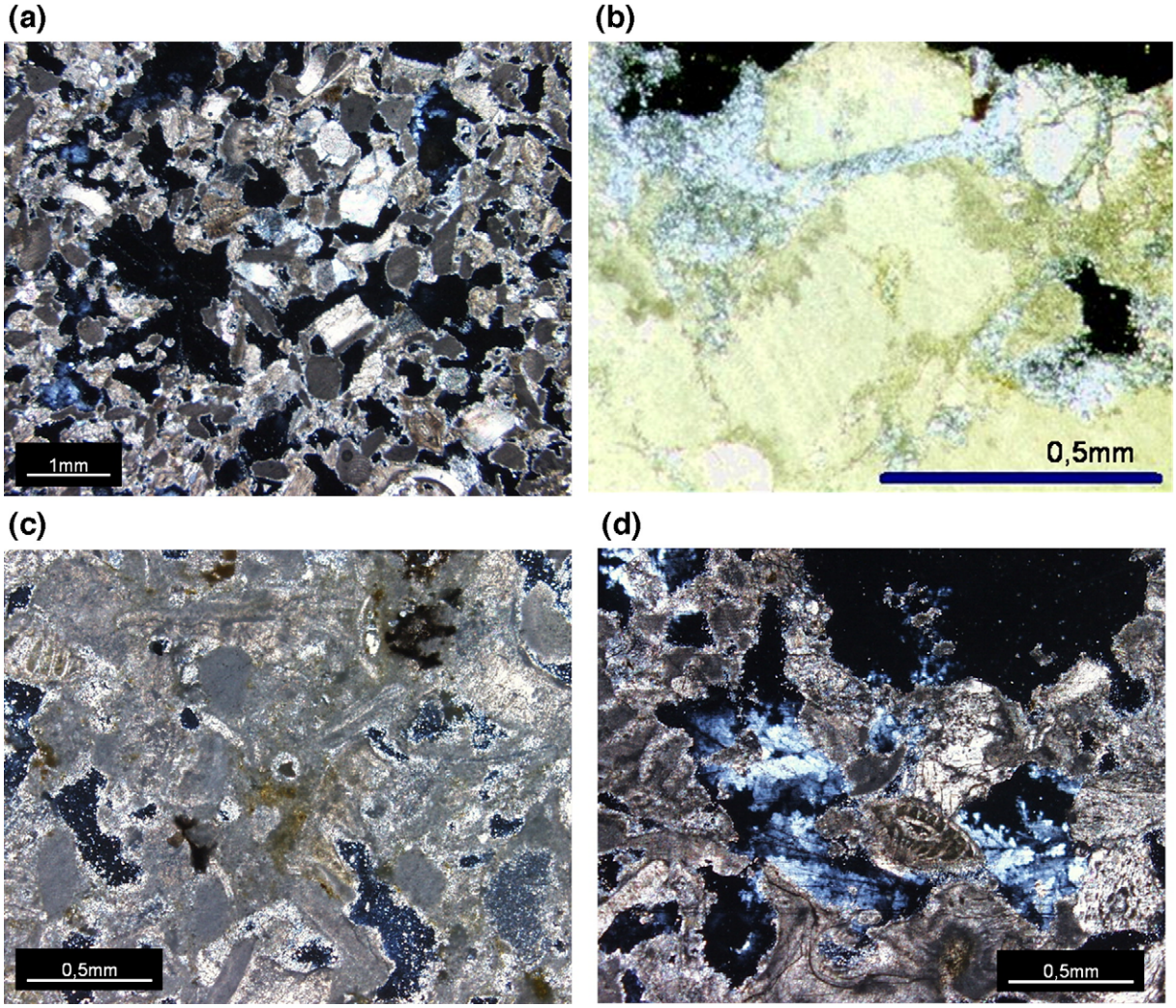

Fig. 3 – Optical microscopy photographs (transmitted light and cross polars) of the calcarenites tested with concentrated solutions: (a) after the action of $MgSO_4·7H_2O$ and $CaSO_4·2H_2O$ solution. Notice the intense dissolution of the carbonate cement; (b) after the action of $MgSO_4·7H_2O$ and $CaSO_4·2H_2O$ solution. Observe the precipitation of Mg-rich salts that break apart the calcarenite in its surface leading to sanding off; (c) after the action of KSO_4 simple solution, showing almost no evidence of physicochemical alteration; (d) after the action of $NaSO_4·10H_2O$ solution. Observe the thenardite crystals showing non-equilibrium needle shapes that correspond to slightly higher supersaturation ratios.

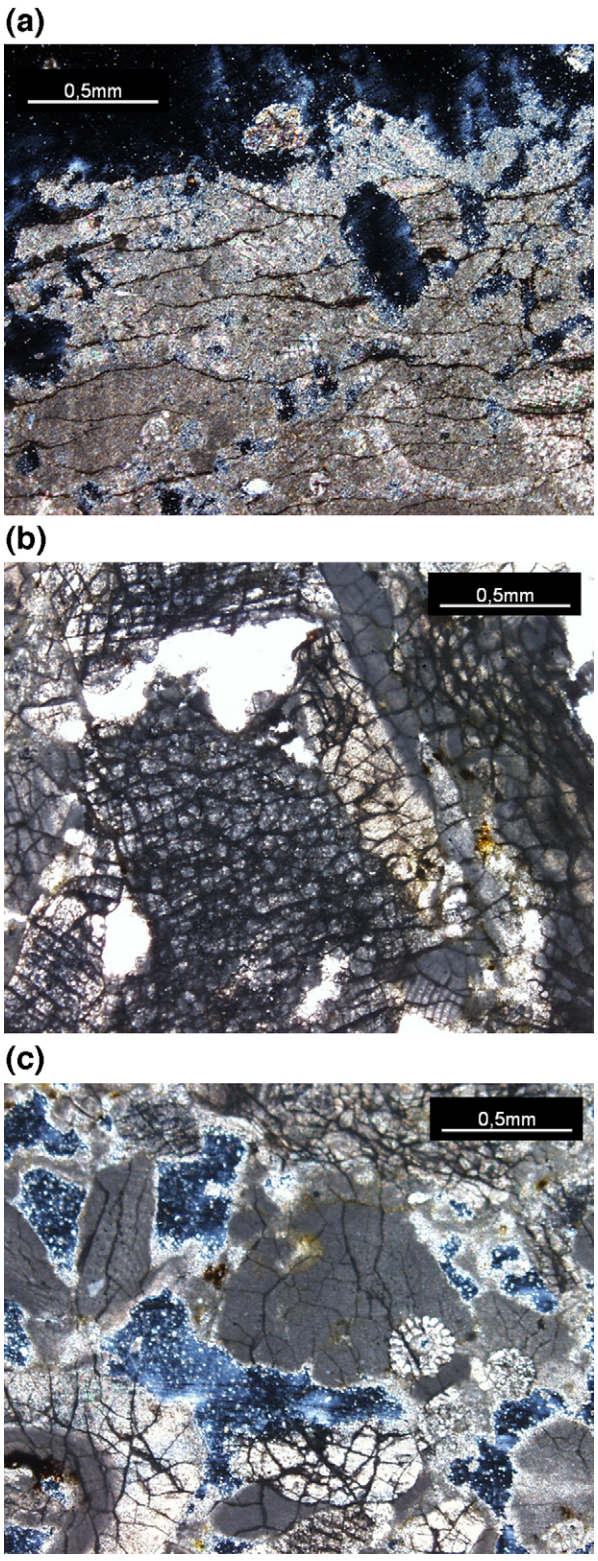

Fig. 4 – Optical microscopy photographs (transmitted light and cross polars) of the calcarenites tested with diluted solutions: (a) after the action of $CaSO_4 \cdot 2H_2O$ solution. Notice the transgranular fissures sub-parallel to the calcarenite surface; (b) after the action of $MgSO_4 \cdot 7H_2O$ and $NaSO_4 \cdot 10H_2O$ solution. Observe the intense intragranular fissuring; (c) after the action of $NaSO_4 \cdot 10H_2O$ solution resulting in cement dissolution, salt crystallization and fissure formation.

Table 9 – Scanning electron microscopy study of the calcarenites tested with the concentrated solutions (#)

#	Sulfate solution	Observations
12	$CaSO_4 \cdot 2H_2O$ + $MgSO_4 \cdot 7H_2O$	Fissures. Cement and bioclast dissolution. Anhedral crystals (<5 μm) made of S, Ca and Mg.
15	$MgSO_4 \cdot 7H_2O$	Fissures. Diverse anhedral crystals (<5 μm) made of *a*=S, Ca and Mg; *b*=S and Mg; *c*=S and Ca.
27	$Na_2SO_4 \cdot 10H_2O$	Cement dissolution. Acicular crystals and anhedral crystals of size <10 μm made of S and Na
42	$MgSO_4 \cdot 7H_2O$ + $Na_2SO_4 \cdot 10H_2O$	Diverse anhedral crystals (<5 μm) made of *a*=Na and S; *b*=Ca and S; *c*=Mg and S.

dissolution of carbonate cement (chemical weathering) (Fig. 3a) and produced few intragranular microfissures (physical weathering). The Mg-rich solutions caused more intense fissuring. The

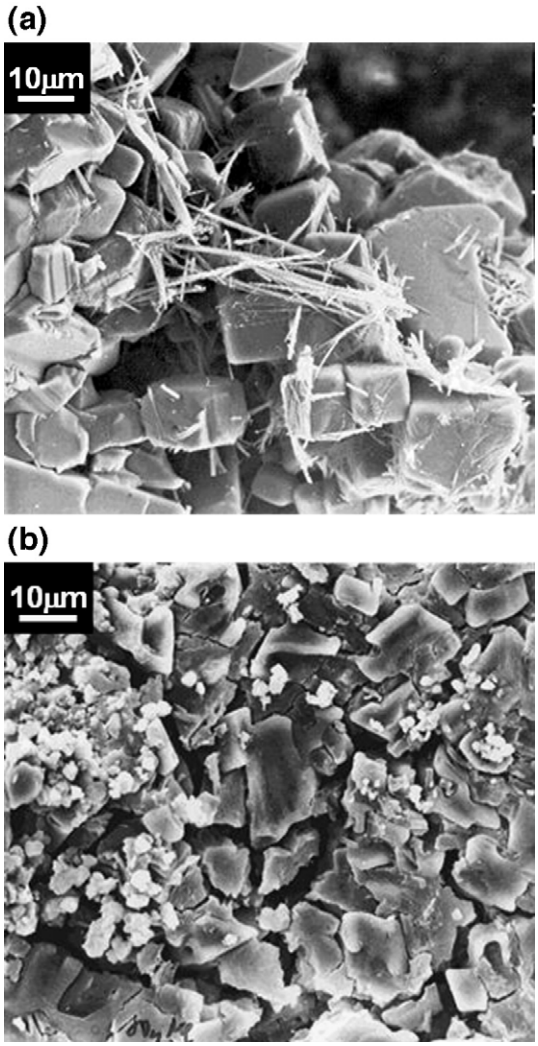

Fig. 5 – SEM micrographs of calcarenites; (a) after the action of the $NaSO_4 \cdot 10H_2O$ solution. Observe the needle-shape of the thenardite crystals and the carbonate cement dissolution of the stone; (b) after the action of concentrated $MgSO_4 \cdot 7H_2O$ and $CaSO_4 \cdot 2H_2O$ solution that provoke intense fissuring in the calcarenite.

mixed solution of Mg and Ca caused salt precipitation near the surface, resulting in sanding off (Fig. 3b). Salt crystallization, cement dissolution and fissuring were less intense in the stones treated with the single solutions of Ca-sulfate and K-sulfate (Fig. 3c). The solutions containing Na caused the most abundant salt precipitation (both subflorescences and efflorescences). The Na-sulfate crystals precipitated as tiny elongated needles grouped in dendrites (Fig. 3d) or as bulky aggregates in both large and small pores. The other salts crystallized as compact anhedral aggregates in different sizes pore.

The diluted solutions caused more intense fissuring than the concentrated solutions. Potassium sulfate caused few intragranular fissures, while Ca-sulfate produced moderate development of transgranular fissures sub-parallel to the calcarenite surface (Fig. 4a). The single solutions of Mg-sulfate and Na-sulfate produced abundant intragranular fissuring, becoming more intense with a mixture of the two single solutions (Fig. 4b). The Ca-sulfate and K-sulfate solutions caused little salt crystallization and low cement dissolution. The solutions rich in Na produced cement dissolution, fissure formation and the highest amount of salts (Fig. 4c). The Mg-sulfate rich solutions caused the most intense fissuring.

3.6. *Scanning Electron Microscopy*

SEM evidence of pore filling is hard to detect. Therefore only 4 samples of calcarenite tested with concentrated solutions were examined (Table 9). The single solution of Mg-sulfate precipitated crystals containing S and Ca interpreted as gypsum, crystals consisting of S and Mg corresponding to Mg-sulfate, and crystals with S, Ca and Mg related to a Ca and Mg double-sulfated salt. The mixed solution of Mg and Ca-sulfates also precipitated a Mg and Ca double-sulfated salt. All the crystals observed were very small (<5 μm). The Na-sulfate crystals grew as anhedral, needle-shaped or bow-tie aggregates (Fig. 5a). In the other cases the crystals were anhedral or subhedral (compact habits). Dissolution of the carbonate cement was observed in the stones treated with the simple solution of Na-sulfate and with a mixed solution of Mg and Ca-sulfates. In this case we also saw dissolution of the carbonate grains and abundant microfissures (Fig. 5b).

3.7. *Pore System*

Fig. 6 shows that the unimodal distribution of the pore radius range in freshly quarried calcarenite (Fig. 6a) was replaced

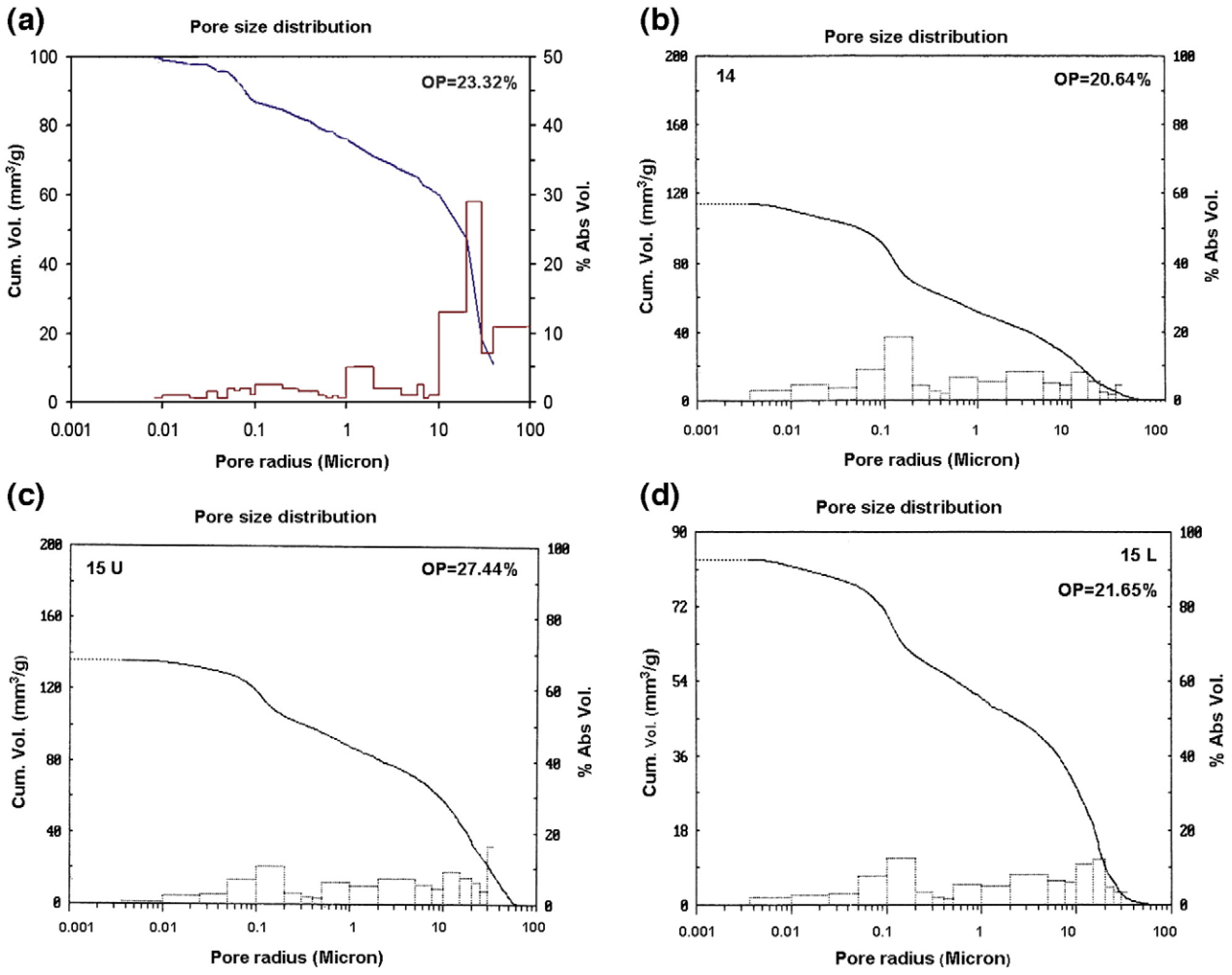

Fig. 6 – Variation of the pore volume related to the pore radii access in fresh quarried calcarenite (a), in calcarenite subjected to the action of dilute $CaSO_4 \cdot 2H_2O$ and $MgSO_4 \cdot 7H_2O$ solution (b), and the action of concentrated $MgSO_4 \cdot 7H_2O$ solution in the lower (c) and in the upper (d) part of the calcarenite.

Table 10 – Total Porosity (TP) and pore (μm) size distribution of fresh and tested calcarenites with sulfate solutions (#)

#	Solutions	TP	Mi	Ma	SA	Pore Size Distribution (%)				
						>10	10–1	1–0.1	0.1–0.01	<0.01
5*	$CaSO_4{\cdot}2H_2O$	21.42	12.10	10.61	2.13	31.63	21.68	27.76	16.98	1.94
9+	$CaSO_4{\cdot}2H_2O$	20.50	9.93	11.22	3.42	41.03	16.50	21.07	16.99	4.40
12*	$CaSO_4{\cdot}2H_2O+MgSO_4{\cdot}7H_2O$	25.52	11.56	15.38	0.97	39.87	25.12	24.35	10.51	0.15
14+	$CaSO_4{\cdot}2H_2O+MgSO_4{\cdot}7H_2O$	20.64	13.46	8.39	2.64	21.44	23.62	34.35	17.72	2.95
15L*	$MgSO_4{\cdot}7H_2O$	21.67	10.93	12.07	1.29	34.01	25.92	24.78	13.39	1.90
15U*	$MgSO_4{\cdot}7H_2O$	27.44	12.07	16.62	1.32	42.75	22.04	22.96	11.74	0.53
19+L	$MgSO_4{\cdot}7H_2O$	26.63	12.88	15.47	1.33	34.57	27.22	24.18	13.60	0.42
19+U	$MgSO_4{\cdot}7H_2O$	25.14	13.88	12.75	1.23	25.52	28.59	31.51	14.22	0.16
27*	$Na_2SO_4{\cdot}10H_2O$	22.79	12.60	12.14	2.41	29.05	27.74	24.71	16.28	2.21
30+	$Na_2SO_4{\cdot}10H_2O$	24.08	12.09	13.31	2.40	35.64	22.82	24.25	15.04	2.24
Esc1	Quarry	23.32	-	-	0.85	60	16	11	12	1
Esc2	Quarry	26.17	-	-	1.03	51	20	13	16	0

TP: correspond to connected open porosity (OP) in %; *: concentrated solutions; +: diluted solutions; =: not analyzed; U: upper part of the block; L: low part of the block; Microporosity in % (radius≤2.5 μm); Ma: Macroporosity in % (radius≥2.5 μm); SA: Surface Area (m^2/g).

after treatment in all the stones by a clearly bimodal pore size distribution, with a maximum in the 0.1–1 μm range and another in the >10 μm range, irrespective of the connected open porosity (OP) of each tested stone. The OP data in freshly quarried and in tested stones (Table 10) suggests that both the fresh and weathered stones were very porous, with little difference between the OP value ranges for the former (23.32–26.17%) and the latter (20.50%–27.44%). After the test the OP fell slightly in the stones tested with concentrated (21.42%) and diluted (20.50%) Ca-sulfate and with the diluted mixture of Ca-sulfate and Mg-sulfate (20.64%). The OP fell in the lower part of the rock treated with concentrated Mg-sulfate (21.67%) and rose in the upper part (27.44%). In the other samples the OP values were similar for fresh and treated calcarenites. The highest volume of pores in the treated stones is concentrated in pores over 10 μm, although the volume is lower than that of the fresh rock (51–60%). The number of spaces concentrated in this pore range decreases especially in stones treated with the diluted mixed solution of Ca-sulfate and Mg-sulfate (21.44%), the Mg-sulfate solution (25.52%) and the concentrated solution of Na-sulfate (29.05%). In all samples the percentage of pores <10 μm increased, except for pores in the 0.1–0.01 μm range whose number was unchanged. The increase in the number of spaces in the <0.01 μm range is noteworthy (particularly after treatment with diluted Ca-sulfate), as to the increase in surface area of the rocks tested with concentrated and diluted solutions of Ca-sulfate (2.13–3.42 $m^2{\cdot}g^{-1}$), Na-sulfate (2.41–2.40 $m^2{\cdot}g^{-1}$) and diluted solution of Ca-sulfate and Mg-sulfate.

4. Discussion

4.1. *Fluid Transport Within the Calcarenites and Related Salt Decay Mechanism*

To explain the fluid transport and salt crystallization alteration mechanisms we must consider the conditions controlling salt precipitation and their location in a porous substratum, which basically depend on: i) the pore system of the material; ii) evaporation conditions and iii) the nature of the saline solution. Since i) and ii) were constant in the experimental conditions of this research, we must attribute the differences observed in the flow dynamics and evaporation of the solutions to their different physical properties, i.e. viscosity, density, surface tension and solute concentration.

As mentioned before our salt crystallization test is based on the model by Lewin [24], which considers capillary rise and migration of the saline solution inside a porous material, concentration of the solution by evaporation, followed by crystallization of salts inside (subflorescences) or outside (efflorescences) the substratum. The site where salts crystallize is determined by the dynamic balance between the rate of evaporation (drying speed) from the surface and the rate of resupply of solution to that site. The former is a function of T and RH. The latter is controlled by pore radii and the physical properties of the introduced solution. Recently, Scherer [19] presented a detailed study of the Lewin's test in terms of fluid transport. The analysis shows that subflorescences precipitate when the evaporative flux (i.e. evaporation velocity), J_E, exceeds the capillary flux, J_C, which can be expressed as:

$$J_C = \frac{2\gamma\cos\theta}{h}\frac{k_S}{\eta}\left(\frac{1}{r_{mS}}-\frac{1}{r_L}\right), \quad (1)$$

where γ is the surface tension, θ the contact angle between the liquid and solid, k_S the permeability of the partially saturated network, h the distance of the receded solution from the stone surface, η the viscosity and r_S and r_L respectively the small and large pore radii. Since in our test the pore system of the material and the evaporation conditions were kept constant, and considering relatively similar contact angles and surface tensions of the diluted and concentrated solutions, it seems viscosity is the most important solution property that controls the capillary flux. Thus the capillary rate increases as viscosity of saline solutions decreases. This would explain why all the tested diluted solutions (with lower viscosities than the concentrated solutions) exhibit the fastest fluid transport. Similarly it would justify the faster flow dynamic of the concentrated Na and K solutions compared to the Mg-rich solutions with higher viscosities (Table 2).

As mentioned previously, subflorescences are mainly produced when the capillary flux is smaller than the evaporative flux. Thus, subflorescences are mainly expected in the tests carried out with concentrated solutions and in particular in those tests where Mg-rich solutions were used. This fact would explain the macroscopic and microscopic observations of the blocks treated with diluted solutions, which show that the scarce salt precipitation occurred mainly close to the rock surface, in contrast to the trend of the concentrated solutions that originate abundant subflorescences in addition to efflorescences.

In the first minutes of the test the penetration of the solutions into the calcarenite mainly depends on its pore system and surface tension. In the diluted solutions, capillary forces are clearly predominant in the solution's rise at the start of the test, as shown by the fact that all the blocks were completely wet 15 h into the test. The low ionic concentration of the diluted solutions appears to have assisted this phenomenon, so that we may consider diffusion of the feeding solution to the rock to be negligible, thus justifying the increase in cation concentration measured in the solutions in the crystallizer. Instead concentrated solutions rose through the calcarenite more slowly and to a lower maximum height than the diluted ones. As Eq. (1) shows, the lower velocity of concentrated solution throughout the stones is justified by the fact that capillary flux (J_C) is inversely proportional to viscosity. On the other hand, the lower heights that these solutions reach in the stones are inversely proportional to their densities, according to Jurin's equation:

$$h = \frac{2\gamma\cos\theta}{\rho g r} \quad (2)$$

where γ is the surface tension, θ is the contact angle between the liquid and solid, ρ is the density, g is the gravitational acceleration and r is the pore radii. The density of the concentrated solutions was estimated. To this end an ion interaction model for the volumetric properties of natural water was used [26]. The following values were obtained for the next solutions: $Na_2SO_4{\cdot}10H_2O = 1.04$ g cm^{-3}; $K_2SO_4 = 1.09$ g cm^{-3}; $MgSO_4{\cdot}7H_2O = 1.30$ g cm^{-3}, $MgSO_4{\cdot}7H_2O + Na_2SO_4{\cdot}10H_2O = 1.18$ g cm^{-3}. This explains why the maximum height in the blocks is attained by $Na_2SO_4{\cdot}10H_2O$ and K_2SO_4 solutions, in contrast to the lowest height reached by the $MgSO_4{\cdot}7H_2O$ solutions.

In this study, we found the blocks dried slowly after treatment with concentrated solutions, and quickly in the case of diluted solutions. The macroscopic and microscopic examination of the calcarenite treated with diluted solutions also showed that almost all solution in the crystallizer was consumed and only scarce precipitation of subflorescences occurred in large pores. Given that similar evaporation conditions were imposed in all the tests, this reveals that the faster drying of blocks treated with diluted solutions should have been assisted because the cohesive forces of the diluted solutions are lower than in the denser, more viscous concentrated solutions (Raoult's law).

As for the stones treated with concentrated solutions, two trends were identified for the crystallization mechanism, leading to i) precipitation mainly of subflorescences and ii) massive crystallization of subflorescences and efflorescences. The first case is that of the stones tested with solutions of Mg, Ca, and a mixture of Mg and Ca-sulfates, where hardly any solution was consumed in the crystallizer. The higher viscosity of these solutions compared to the diluted solutions hinders their migrating to higher parts of the block. Both the large and small pores of the lower parts of these blocks filled with salts, preventing evaporation and so no more solution was consumed from the crystallizer. In addition, the sealing of the pores with salts seems to be a self-limiting weathering factor, causing a change in the system dynamics resulting in a gradual reduction of deterioration. The effect of the salts "blocking" the pores would be similar to the "hardening" of the surface in natural outcrops and monuments, leading to a state of "self-conservation" of the porous material [27]. The second case is that of the calcarenite treated with simple solutions of Na and K-sulfate, which were totally consumed in the crystallizer. Massive precipitation of subflorescences and efflorescences occurs at different heights, including the top. The lower viscosity of these solutions in comparison to the Mg- and Ca-rich solutions is responsible for this, providing higher flow dynamics that allow them to reach the surface of the stone.

The presence of Ca^{2+} in the solutions in the crystallizer and the lack of variation in its concentration can be explained by the compensation of the two phenomena acting on the calcarenite, as showed by OM and SEM-EDX results. On the one hand, there is dissolution of the carbonate cement under the corrosive action of the solutions (with acid pHs) and, on the other, gypsum and Ca-rich double-sulfated salts precipitate. The increase in Ca^{2+} concentration detected in the diluted solutions can be explained because the action of the feeding solutions only causes dissolution of the cement, but not precipitation of Ca salts in the stone.

4.2. *Calcarenite–brine Interaction: Decay Forms and Weathering Mechanisms*

Because of salt crystallization, the stones tested with concentrated solutions increased in mass after the test. However, those treated with diluted solutions maintained their initial mass or showed only a slight increase, indicating little or no salt precipitation. Naked-eye examination of the blocks treated with both concentrated and diluted Na-solutions found abundant efflorescences and loss of material through sanding off. The compensation between both phenomena explains the lack of variation in sample mass.

Efflorescences only precipitated in the calcarenite treated with concentrated solutions. The efflorescences crystallize as crusts, whiskers and powdery salts. A crystal's habit and manner of growth are controlled by internal and external factors [28], of which the latter are particularly interesting in the context of monument conservation [14]. Despite the strong influence of T and RH on crystal habit, the key external factor in the growth morphologies is the humidity of the porous substratum and the type of solution supply [14]. In our case, the continuous supply of solution to the stone and the high saturation of the solutions tested explain why all the efflorescences precipitated as granular crusts. The crusts were harder and thicker on the lower parts of the blocks, which were very wet due to the abundant solution supply, changing

to a fine, occasionally fibrous film on the upper, less moist parts. Although the crusts normally form from not very soluble salts, such as calcite ($CaCO_3$), gypsum ($CaSO_2{\cdot}2H_2O$) or nesquehonite ($MgCO_3{\cdot}3H_2O$), any salt can precipitate as crust under suitable conditions like those of this test. Moreover, in accordance with the high concentrations here used, no crystals with equilibrium morphologies indicative of low degrees of saturation were observed [28].

The presence of mineral phases such as gypsum, nesquehonite and Ca-Mg double salt in the crusts precipitated from Mg-rich solutions must be the result of the dissolution of the carbonate cement and precipitation of salts through chemical reaction in the calcarenite. These results, confirmed by SEM-EDX and OM, show that the Mg-rich solutions cause more intense chemical weathering on the calcarenite than the other solutions. Moreover, the crystallization of anhydride or less hydrated mineral phases than those introduced into the stone, e.g. crystallization of thenardite and hexahydrite from mirabilite and epsomite solutions respectively, is determined by the degree of saturation of the solutions. Indeed, an increase in concentration of a saline solution significantly reduces the activity of the water, making the anhydride phase the most stable, regardless of the RH [18].

The naturally occurring members of the $MgSO_4{\cdot}nH_2O$ series are epsomite ($MgSO_4{\cdot}7H_2O$), hexahydrite ($MgSO_4{\cdot}6H_2O$) and kieserite ($MgSO_4{\cdot}H_2O$). According to García-Ginea et al. [29] and Cardell et al. [30], epsomite transforms to hexahydrite above 28 °C. Vaniman et al. [31] found that epsomite transforms readily to hexahydrite below ~50–55% at ~25 °C. Given that the RH of the test was maintained below 40%, it was to be expected that only hexahydrite would precipitate, but the XRD results showed that epsomite also precipitated. It is known that the transition RH values of pure salts decrease in the presence of other soluble salts [32]. The chemical reaction between the cement and the solutions, observed under OM and SEM, must have supplied new solutes to the starting solutions for this phenomenon to happen.

Regarding the other habits observed in the salts, we only identified thenardite and arcanite whiskers. These crystallized in substrata with very little humidity from low saturation solution, which explains their appearance in the upper parts of the blocks and/or on previous crusts or at the end of the test. The whiskers growing on the crusts are long, very fine and twisted, since the crust surface is denser than that of the calcarenite and the evaporation rate is somewhat lower. On the other hand, loose aggregates of thenardite only formed 67 h after the start of the test, suggesting that the salt had aged. Variation of a crystal's habit over time is possible since salts constitute a dynamic system in which transformations are constantly taking place [33]. This aging trend has also been observed in efflorescences growing on actual monuments. Thus Zehnder and Arnold [14] found that the acicular growth of a nitratite turned into a more isometric shape with time, and Cardell [12] observed a similar evolution in epsomite crystals. The evolution in space and time of the habits of only the Na-sulfate efflorescences, in the surprisingly short interval of 3 h, illustrates the rapid dynamics of the crystallization and transformation of this salt in comparison with the other sulfates tested. This may therefore be a key factor in the harmful action of this salt, to judge by the deterioration observed.

The crystallization behavior of Na-sulfate crystals is rather complex, with many studies of the subject providing sometimes contradictory results, thus adding to the controversy [7,30,34]. The Na_2SO_4–H_2O system includes two stable phases at room T. In equilibrium conditions and according to the literature, these phases are thenardite (Na_2SO_4), an anhydride phase that precipitates directly from the solution above 32.4 °C, and mirabilite ($Na_2SO_4{\cdot}10H_2O$), which is stable below that T, with mirabilite dehydrating rapidly when RH falls below 71% (20 °C) [18,35].

In this test carried out in room conditions of 18–30 °C and RH <40%, the only phase identified by XRD and SEM-EDX was thenardite. We should make clear that we only analyzed salt composition at the end of the test and so it is not known whether mirabilite precipitated during its course. However, considering the high rate of evaporation and the high supersaturation of the solution tested, implying a decrease in water activity thus encouraging precipitation of the anhydride phases, we can reasonably assume that the salt directly precipitated from the solution would have been thenardite. Moreover, the growth morphologies observed by OM and SEM confirm this assumption (Fig. 3d), as none correspond to the shapes typically observed after dehydration of mirabilite [7]. The SEM analyses show that the thenardite grows as anhedral, needle-shaped or bow-tie aggregates, shapes corresponding to crystals formed in very high supersaturation conditions. These results agree with those obtained by other authors [7,12] for thenardite precipitation in experimental conditions of high supersaturation ratios, T below 34 °C and high evaporation due to low RH (40% approx.). Heterogeneous nucleation of thenardite seems to be the kinetic reason for its formation below the mirabilite–thenardite transition T. In addition, the reduction of energy necessary for formation of stable thenardite nuclei appears to be sufficient to prevent mirabilite formation, with the necessary condition of high supersaturation ratios [7]. Moreover, salt precipitation in small pore radii under environment conditions of low RH encourages high capillary pressure, which in turn decreases water activity thus driving thenardite precipitation.

To understand the mineral precipitation from multicomponent concentrated solutions, a theoretical simulation of the evaporation process was carried out using the PHRQPITZ geochemical code [36], which applied the Pitzer virial coefficient approach for activity coefficient corrections. The evaporation process is simulated by the removal of water from the initial solution until a mineral phase precipitates. In this situation, the saturation index, SI, is equal to zero, and it is defined as the logarithmic ratio of the ionic activity product to equilibrium constant of the considered mineral. The simulation was performed at 25 °C (isothermal evaporation) for those solutions whose interaction with the calcarenite originated the most diverse salt compositions (Table 7). These solutions are $MgSO_4{\cdot}7H_2O + Na_2SO_4{\cdot}10H_2O$ (no. 42) and $MgSO_4{\cdot}7H_2O$ (no. 15). We have considered that the solutions were in equilibrium with respect to calcite, since the presence of Ca^{2+} in the solutions comes from the dissolution of carbonate cement. This thermodynamic approximation is consistent with the efflorescences identified by XRD in the calcarenite blocks, as shown in Table 7.

Thus, the initial ionic composition for the most complex solution $MgSO_4{\cdot}7H_2O + Na_2SO_4{\cdot}\ 10H_2O$ was: $4.83{\cdot}10^{-3}$ m Ca^{+2}; 1.47 m Mg^{+2}; $3.49{\cdot}10^{-1}$ m Na^{+}; $4.83{\cdot}10^{-03}$ m CO_3^{-2}; 1.65 m SO_4^{-2}. Two-steps reactions can be described to explain the saline mineral precipitation sequence observed on this test: (1) epsomite + hexahydrite precipitation, (2) epsomite + hexahydrite + thenardite precipitation. In step (1), water is removed from saline solution to reach hexahydrite precipitation. In this situation, hexahydrite is then saturated (SI = 0.000); epsomite is slightly supersaturated (SI = 0.174); and gypsum is also supersaturated (SI = 0.537), which explains the formation of the latter. In step (2), water is removed from the latter solution to reach thenardite precipitation. In this situation, thenardite and hexahydrite are then saturated (SI = 0.000); epsomite is also supersaturated (SI = 0.140); however mirabilite is roughly sub-saturated (SI = −0.136), which explains the greater thenardite precipitation although small amounts of mirabilite crystals may be also crystallized. When thenardite crystals precipitate, water activity is equal to 0.7836, and consequently, the RH in equilibrium with this saline solution will be 78.36%. Given that the environmental RH of the test was maintained below 40%, a massive saline precipitation is expected. Regarding the $MgSO_4{\cdot}7H_2O$ solution (no. 15), the calculated initial ionic composition was: $7.04{\cdot}10^{-3}$ m Ca^{+2}; 3.02 m Mg^{+2}; $7.04{\cdot}10^{-3}$ m CO_3^{-2}; 3.02 m SO_4^{-2}. The saline mineral precipitation sequence observed during this test can be described as the following one-step reaction. Water is removed from the saline solution causing hexahydrite precipitation. In this situation, hexahydrite is then saturated (SI = 0.000); epsomite is slightly supersaturated (SI = 0.185); and gypsum is also supersaturated (SI = 0.428). Additionally, other efflorescences identified by XRD arising from the action of this solution on the calcarenite correspond to Mg-carbonates (Table 7), which may range from magnesite (SI = 2.303) to nesquehonite, which is close to saturation (SI = −0.545) and is expected to precipitate due to the low experimental RH.

The OM study reveals that in blocks treated with diluted solutions, salts precipitate preferentially in larger pores, which must have contributed to damage being minimal. Macropores provide sinks for high supersaturations by growth of large crystals that would not develop sufficiently large stresses to damage the calcarenite [17]. This result is consistent with the fact that high supersaturation is needed for crystallization to occur in the smaller pores, conditions not reached in the diluted solutions used in the test. On the other hand, the tensile strength of the calcarenite was exceeded in the samples treated with concentrated solutions, considering the sanding off and bursting observed by the naked eye. In these cases, OM and SEM analyses showed that the salts precipitated in pores of different sizes, including smaller ones, even when large pores had not been completely filled with salt. Crystallization of salts in small pores is the phenomenon capable of causing pressures high enough to cause breakage of the host material [1,37]. Similar results have been obtained elsewhere [7,12,38]. A possible explanation is the heterogeneous nucleation of crystals caused by the proximity to the narrow connection channels between large and small pores that could act as a surface defect [38]. For the case of thenardite, a very high supersaturation of the pore solution has been invoked to explain its heterogeneous nucleation [7]. However this hypothesis seems not feasible because heterogeneous nucleation requires less saturation than does homogeneous nucleation due to lower activation energy requirements [18].

On the other hand, our results reveal that all sulfate solutions, irrespective of their concentration and composition, provoke microfissures in the calcarenites. Nevertheless microfissures were more abundant when diluted solutions were introduced in the stones than when concentrated solutions were used. It should be recalled that diluted solutions originate scarce subflorescences whereas concentrated solutions lead to abundant precipitation of both subflorescences and efflorescences. Microcracking is highly dependent on the mineralogy, fabric, and microstructure of a given rock type [39]. We propose that the presence of subflorescences could be a limiting factor in microfissure coalescence and propagation. In fact, this argument would justify the absence of visually observed fissures in the lower part of the block tested with concentrated Mg-sulfate, in comparison with the upper part where abundant cracks are seen but efflorescences are not. The hypothesis that subflorescences can increase to some extent the stone´s resistance to brittle deformation could be explained by the fact that salts are more flexible than the calcarenite forming minerals (i.e. calcite, quartz, feldspars and clays).

4.3. *Binding or Disintegrating Effects of Sulfates on the Calcarenite*

Analysis of the alterations to the pore system in a material affected by salt crystallization allows identification of its deterioration mechanisms [1,11]. Decrease in total porosity (i.e. connected open porosity) must be the result of salts filling the spaces, which implies a binding effect. On the other hand, an increase in total porosity could be due to several phenomena, such as cement dissolution, fissuring, etc., possibly leading to breakage and loss of matter. In the present study, the solutions causing most binding were the concentrated solutions of Ca-sulfate, Mg-sulfate (only in the lower parts of the blocks) and Na-sulfate, since their action on the calcarenite caused the greatest decrease in total porosity, due to the precipitation of subflorescences. The Mg-sulfate solution also caused an increase in total porosity in the upper part of the stone. It was observed that in this area the calcarenite took on a brownish-orange tone where it fractured and burst, possibly related to the local presence of clays. Decay may be further accelerated through the swelling of clays promoted by the presence of salts [40]. In the other samples, the general trend of no variation in total porosity does not agree with the evidence of decay and can only be explained by the compensation of porosity caused by fissuring and cement dissolution and the decrease in porosity due to salts filling the spaces.

Analyses of pore modifications due to salt weathering indicated that a variety of mechanisms could be responsible for change of the pore structure. In all cases the significant decrease in volume of >10 μm pores shows that salts precipitated preferentially here, which implies and explains the increase in pores in the 10–1 μm and 1–0.1 μm ranges. In this study, the simple concentrated solution of Na-sulfate, the simple diluted solution of Mg-sulfate in the lower parts of the sample and the mixed diluted solution of Ca and Mg-sulfate caused most salt precipitation in the largest spaces. Although

the increase in the smallest pores (<0.01 μm) can be explained by the partial filling of larger spaces with salts, OM and SEM examination showed many new fissures of <1 μm (Fig. 4c) and dissolution of carbonate cement, both of which create new void space. The new distribution of the pore system, with a substantial increase in micropore volume and, therefore, an increase in surface area, make the calcarenite more vulnerable to auto-feedback processes.

To properly apply the ultrasonic transmission technique as an efficient tool to evaluate the degree of alteration caused by salt crystallization in stones, comparison between the ultrasonic speed values of fresh stones and those of deteriorated stones have to be performed. Typically, salts are removed previously from the altered stones using distilled water. By contrast, in this work the ultrasonic transmission technique was applied to the altered stones without extracting the salts, although it was indispensable to scrape the efflorescences to have good connection between the sensors and the stone. In other words, subflorescences still remain inside the stones. The aim was to evaluate the binding or disintegrating effect of the different sulfate solutions on the stones. In our judgment this procedure better reflects the reality operating in situ in buildings. In fact, when this technique is applied in situ to evaluate the deterioration state of an artifact that can load soluble or crystallized salts, it is not the common procedure to extract the salt content from it because of the difficulty of the process. Therefore it is interesting to characterize the effect of salts precipitated inside the porous media on the speed of the ultrasonic waves.

The slight fall in ultrasound speeds in the stone treated with concentrated K-sulfate can be explained by the increase in porosity due to the cement dissolution and fissuring, and the fact that subflorescences are scarce. It should be remembered that this solution caused mainly precipitation of efflorescences that, as mentioned above, were removed to perform the ultrasonic measurement. Regarding the data measured in the stones treated with diluted solutions, which were similar to the values found before the test, they can only be explained by the compensation between the effect of fissure generation and the precipitation of subflorescences. The maintenance of ultrasound speeds in no case implied an improvement of the stone's mechanical properties. In our test the lack of coherent ultrasonic response in the blocks with massive efflorescences, cracks and sanding off requires no explanation.

Other authors have pointed out the paradoxical invariability or increase in ultrasound speeds after subjecting limestones to a salt crystallization test, proposing a critical revision of the test, but without providing a reason for the cause of the improvement [41]. Our results suggest that this improvement is due to the binding action of the subflorescences, which also implies the need to reconsider the effect of subflorescence crystallization on a porous material, which is traditionally and systematically considered in the literature to be very destructive. In recent years there has been discussion of the binding or disintegrating effects of crystallized salts in a porous substratum. Until now, these effects have been related to the location of salt crystallization, so that subflorescences would cause severe damage when precipitated inside the host (disruptive effect) whereas efflorescences would only affect the aesthetic appearance of the object [24]. Our results show that the moderate development of subflorescences from weakly saturated solutions causes a binding effect in the calcarenite, whereas subflorescence precipitation from highly concentrated saline solutions has a disintegrating effect leading to break up of the stone.

5. Conclusions

The obtained results, representing basic information for building and monument conservation, are summarized as follows:

1. Fluid transport within the stone is determined by solution concentration. Subflorescences precipitate when the evaporative flux is greater than the capillary flux, which is mainly controlled by solution viscosity. Thus, the capillary rate increases as viscosity of saline solution decreases. With diluted solutions, salts precipitate mainly close to the rock surface and with concentrated solution plentiful subflorescences and efflorescences occur, in particular with Na-rich solutions.
2. All sulfate solutions lead to physical and chemical weathering depending on saturation rates. For dilute solutions, although macroscopic deterioration was not evident, chemical and particularly physical weathering processes affect the limestone (intense microfissures). Magnesium-rich solutions cause the most intense chemical weathering.
3. Concentrated solutions cause the most intense damage through precipitation of subflorescences and efflorescences, dissolution of carbonate cement and clasts and weak fissuring. Sodium-rich solutions lead to massive precipitation of both subflorescences and efflorescences, which generate granular disaggregation. By contrast, Mg-rich solutions produce a decay mechanism based principally on the generation and propagation of microfissures that result in macroscale cracks. Calcium- and K-rich solutions cause moderate precipitation of subflorescences that do not result in intense damage.
4. Microfissuring is highly dependent on the solution composition and the presence of subflorescences. The fact that microfissures are less intense when abundant subflorescences precipitate suggests that this process makes fissure coalescence and propagation more difficult.
5. Simple solutions cause more damage than do mixed solutions. The most damaging solutions are simple Na and Mg solutions, followed by mixed Mg and Ca solutions.
6. Salt crystallization pressure is responsible for physical weathering of the stone, since no salt hydration processes operated in the low relative humidity conditions of this test.
7. Subflorescences do not inevitably lead to critical stone decay, which rather is controlled by the supersaturation rate of the solution from which the salt precipitates. Thus, dilute solutions led to moderate precipitation of subflorescences in larger pores causing a binding effect, since their low concentrations do not trigger high crystallization pressures. On the other hand, concentrated solutions promote massive subflorescences in both coarse and small pores, causing a disrupting effect that ultimately break down the stone.

Acknowledgements

Financial support for this work was provided by the Andalusian Research Group RNM-0179 and a post-doctoral research contract from the Junta de Andalucia awarded to C. Cardell. We thank the Scientific Instrumentation Centre (CIC) of the University of Granada for the SEM-EDX analyses, and the "Gino Bozza" Research Center (Milan, Italy) for the Mercury Porosimetry Analysis.

REFERENCES

[1] Cardell C, Delalieux F, Roumpopoulos K, Moropoulou A, Auger F, Van Grieken R. Salt induced decay in calcareous stone monuments and buildings in a marine environment in SW France. Constr Build Mater 2003;17:165–79.
[2] Doehne E. Salt weathering: A selective review. In: Siegesmund GS, Vollbrecht A, Weiss T, editors. Natural stone, weathering phenomena, conservation strategies and case studies. London: Geological Society; 2003. p. 205–19.
[3] Götze J, Siedel H. Microscopic scale characterization of ancient building sandstones from Saxony (Germany). Mater Charact 2004;53:209–22.
[4] Coussy O. Deformation and stress from in-pore drying-induced crystallisation of salt. J Mech Phys Solids 2006;54:1517–47.
[5] Charola AE. Salts in the deterioration of porous materials: an overview. J Am Inst Conserv 2000;39:327–43.
[6] Cardell C, Yebra A, Van Grieken R. Applying digital image processing to SEM-EDX and BSE images to determine and quantify porosity and salts with depth in porous media. Microchim Acta 2002;140:9–14.
[7] Rodríguez-Navarro C, Dohene E, Sebastián-Pardo E. How does Na sulfate crystallize? Implications for the decay and testing of building materials. Cem Concr Res 2000;30:1527–34.
[8] Pel L, Huinink H, Kopinga K. Ion transport and crystallization in inorganic building materials as studied by nuclear magnetic resonance. Appl Phys Lett 2002;81-15:2893–5.
[9] Cardell C, Rivas T, Mosquera MJ, Birginie JM, Moropoulou A, Prieto B, et al. Patterns of damage in igneous and sedimentary rocks under conditions simulating sea-salt weathering. Earth Surf Process Landf 2003;28-1:1–14.
[10] Rivas T, Prieto B, Silva B, Birginie JM. Weathering of granitic rocks by chlorides: effect of the nature of the solution on weathering morphology. Earth Surf Process Landf 2003;28-4:425–36.
[11] Benavente D, García del Cura MA, Bernabeu A, Ordóñez S. Quantification of salt weathering in porous stones using an experimental continuous partial immersion method. Eng Geol 2001;59:313–25.
[12] Cardell C. Salt crystallization in calcarenites: application to the monastery of Sant Gerome, Granada (Spain). Ph.D. Thesis, The University of Granada, Granada, Spain; 1998 (in Spanish).
[13] Selwitz C, Doehne E. The evaluation of crystallization modifiers for controlling salt damage to limestone. J Cult Herit 2002;3-3:205–16.
[14] Zehnder K, Arnold A. Crystal growth in salt efflorescence. J Cryst Growth 1989;97:513–21.
[15] La Iglesia A, González V, López-Acevedo V, Viedma C. Salt crystallisation in porous construction materials I. Estimation of crystallization pressure. J Cryst Growth 1997;177:111–8.
[16] Steiger M, Zeunert K. Crystallisation properties of salt mixtures: comparison of experimental results and models calculations. Proc Int Congr on Deterioration and Conservation of Stone. Berlin, Germany, September 30 - October 4; 1996.
[17] Flatt RJ. Salt damage in porous materials: how high supersaturations are generated. J Cryst Growth 2002;242:435–54.
[18] Benavente D, García del Cura MA, García-Guinea J, Sánchez-Moral S, Ordoñez S. Role of pore structure in salt crystallisation in unsatured porous stone. J Cryst Growth 2004;260:532–44.
[19] Scherer GW. Stress from crystallization of salt. Cem Concr Res 2004;34:1613–24.
[20] Steiger M. Crystal growth in porous materials — I: the crystallization pressure of large crystals. J Cryst Growth 2005;282:455–69.
[21] López-Acevedo V, Viedma C, González V, La Iglesia A. Salt crystallization in porous construction materials II. Mass transport and crystallization processes. J Cryst Growth 1997;182:103–10.
[22] Mosquera MJ, Rivas T, Prieto B, Silva B. Capillary rise in granitic rocks: interpretation of kinetics on the basis of pore structure. Colloid Interface Sci 2000;222:41–5.
[23] Sebastián E, Zezza U, Rodríguez Navarro C, De la Torre MJ, Cardell C. La piedra franca (biocalcarenita) en la construcción de monumentos históricos de Granada (España). Proc Int Congr on Rehabilitation of Architectonic and Building Heritage. Tenerife, Spain, June 2-6; 1992.
[24] Lewin SZ. The mechanism of masonry decay through crystallization. In: Barkin SM, editor. Conservation of Historic Stone Building and Monuments. Washington DC: National Academy of Science; 1981. p. 120–44.
[25] NORMAL 22/86. Misura della velovitá di propagazione del suono. Roma: CNR-IC; 1987. 7 pp.
[26] Monnin C. An ion interaction model for volumetric properties of natural waters: density of the solution and partial volumes of electrolytes to high concentrations at 25 °C. Geochim Cosmochim Acta 1989;53:1177–88.
[27] Delalieux F, Cardell C, Todorov V, Dekov V, Van Grieken R. Environmental conditions controlling the chemical weathering of the Madara Horseman monument, NE Bulgaria. J Cult Herit 2001;2:43–54.
[28] Sunagawa I. Characteristics of crystal growth in nature as seen from the morphology of mineral crystals. Bull Mineral 1981;104:81–7.
[29] García-Ginea J, Abella R, Sánchez-Moral S, Benito R, Martín-Ramos D. Examining hydrated minerals using optically stimulated X-ray diffraction, an inexpensive modification of traditional diffractometers. J Sediment Res 2000;7-4:964–7.
[30] Cardell C, Sánchez-Navas A, Olmo-Reyes FJ, Martín-Ramos JD. Powder X-ray thermodiffraction study of mirabilite and epsomite dehydration. Effects of direct IR-irradiation on samples, vol. 79. Anal Chem; 2007. p. 4455–62.
[31] Vaniman DT, Bish DL, Chipera SJ, Fialips CI, Carey JW, Feldman WC. Mg sulfate salts and the history of water on Mars. Nature 2004;43:663–5.
[32] Price CA, Brimblecombe P. Preventing salt damage in porous materials. In: Roy A, Smith P, editors. Preventive conservation: practice, theory and research. London: International Institute for Conservation of Historic and artistic works; 1994. p. 90–3.
[33] Doehne E. ESEM applications: from cultural heritage to nano-behaviour. Conservation. Microchim Acta 2006;155:45–50.
[34] Tsui N, Flat RJ, Scherer GW. Crystallization damage by Na sulfate. J Cult Herit 2003;4:109–15.
[35] Charola AE, Weber J. The hydration-dehydration mechanism of Na sulfate. Proc Int Congr on Deterioration and Conservation of Stone. Lisbon, Portugal, June 15-18; 1992.
[36] Plummer LN, Parkhurst DL, Fleming GW, Dunkle SA. A computer program incorporating Pitzer's equations for calculation of geochemical reactions in Brines. USGS. Water Res Inv 1988;88:41–53.
[37] Rossi-Manaresi R, Tucci A. Pore structure and the disruptive or cementing effect of salt crystallisation in various types of stone. Stud Conserv 1991;36:53–8.

[38] Dei L, Mauro M, Baglioni P. Growth of crystal phases in porous media. Langmuir 1999;15:8915–22.
[39] Åkesson U, Hansson J, Stigh J. Characterisation of microcracks in the Bohus granite, western Sweden, caused by uniaxial cyclic loading. Eng Geol 2004;72:131–42.
[40] McGreevy JP, Smith BJ. The possible role of clay minerals in salt weathering. Catena 1984;11:169–75.
[41] Calleja L, Montoto M, Pérez-García B, Suárez del Río LM, Martínez Hernando A, Menéndez-Villar B. An ultrasonic method to analyse the progress of weathering during cyclic salt crystallization laboratory test. Proc Int on Monument Conservation in the Mediterranean Basin. Bari, Italy, July 7-10; 1989.
[42] Lide DR, (Ed.). CRC Handbook of Chemistry and Physics, Boca Raton, London, NY, Washington, DC: CRC Press; 1998.
[43] Lide DR, (Ed.). CRC Handbook of Chemistry and Physics, Boca Raton, London, NY, Washington, DC: CRC Press; 2003.